Geophysical Research Letters

Supporting Information for

Preparatory Slip in Laboratory Faults: Effects of Roughness and Loading Rate

Simon Guérin-Marthe[1], Grzegorz Kwiatek[1], Lei Wang[1], Audrey Bonnelye[1,2], Patricia Martínez-Garzón[1], Georg Dresen[1,3]

[1]Helmholtz Centre Potsdam, GFZ German Research Centre for Geosciences, Section 4.2 Geomechanics and Scientific Drilling, Potsdam, Germany.
[2]Free University Berlin, Berlin, Germany
[3]University of Potsdam, Potsdam, Germany

Contents of this file

Introduction

The complementary material of the article includes:

- The description of Acoustic Emissions (AEs) processing (Text S1)
- The roughness characterization of the fault surfaces (Fig. S1)
- The sensor setup (Fig. S2)
- The scans of the sandblasted sawcut surfaces (Fig. S3)
- The acoustic emission locations prior a stick-slip event, superimposed to the topography of the rough fault (Fig. S4)
- Stress vs strain curve for estimating the Young's modulus of the La Peyratte granite samples. (Fig. S5)
- The stress, slip and strain evolution during a few seconds prior to selected stick-slip events on rough and smooth faults (Fig. S6)
- The fault stiffness estimation (Fig. S7)
- A zoom on stick-slip events on the rough fault, with the acoustic emission locations (Fig. S8)
- The b-value evolution during the experiment on the rough fault (Fig. S9)
- The relation between stress drop and maximum slip velocity (Fig. S10)
- A comparison between the slip velocity during the preparatory phase of smooth faults and the load point velocity (Fig. S11)

Text S1.

Full AE waveforms, as well as active ultrasonic transmission measurements were recorded at a sampling rate of 10 MHz with 16-bit amplitude resolution using the 16-channels DAXBox (Prökel) recording system. The full waveform recordings were first separated into AE events and UT measurements using an automated procedure. Active ultrasonic transmission (UT) measurements were performed every 10 seconds throughout the whole experiment. P-wave travel times were first picked using the Akaike information criterion (AIC) criterion and corrected for the sample deformation and fault slip. These travel times were then used to calculate time-dependent quasi-anisotropic *P*-wave velocity model composed of 5 layers perpendicular to and 1 vertical layer parallel to loading axis (see e.g., Stanchits et al. 2011; Kwiatek et al. 2014). The recordings of AE events were first amplified by 40 dB and high-pass filtered at 100 kHz (Physical Acoustic Corporation). *P*-wave arrival times were automatically picked using the convolutional neural network-type picker based on Ross et al., (2018) picker trained on AE experiments. To locate AEs, the Equivalent Differential Time method (e.g., Font et al., 2004) was used and solved using a combination of grid search followed by simplex (e.g. Nelder and Mead, 1965) optimization algorithms while using the time-dependent velocity model derived earlier from UT data. The average AE hypocenter location accuracy is ± 2 mm (Stanchits et al., 2011).

After hypocenter determination, the relative AE magnitude was estimated as:

$$M_{\mathrm{AE}} = \log_{10} \sqrt{\frac{1}{n} \sum_{i=1}^{n} (A_i R_i)^2},$$

where A_i and R_i are the first P-wave amplitude and source-receiver distance for each individual AE sensor i, respectively (e.g. Dresen et al., 2020; Zang et al., 1998). We note this magnitude reveals relative size differences between AE events and is not directly calibrated to the physical size of the events (see e.g. Dresen et al., 2020 for additional discussion). Finally, polarity coefficient has been calculated for each AE event following Zang et al. (1998):

$$p_{\mathrm{AE}} = \frac{1}{n} \sum_{i=1}^{n} \mathrm{sgn}(A_i),$$

using average polarity of first P-wave amplitudes (cf. Figure S9c). This parameter signifies whether the AE events microkinematics reflects material compaction, tensile opening or shearing (see Zang et al. 1998 for details).

Using the catalog of located AE events above the AE magnitude of completeness of $M_{AE}^{C} = 1.8$ (assessed by visual inspection of magnitude-frequency distribution) we calculated the magnitude-frequency Gutenberg Richter b-value in a moving time window of 200 seconds (Figure S9b). For each window, the b-value has been estimated using the maximum likelihood approach:

$$b = \frac{1}{\overline{M_{\mathrm{AE}}} - M_{\mathrm{AE}}^{C}} \log_{10}(e),$$

where $\overline{M_{AE}}$ is the average magnitude of events above magnitude of completeness. The estimates have been corrected for the bin size (e.g. Guo & Ogata, 1997). The uncertainties of *b*-value have been estimated following Shi & Bolt (1982), suitable for weakly non-stationary catalogs.

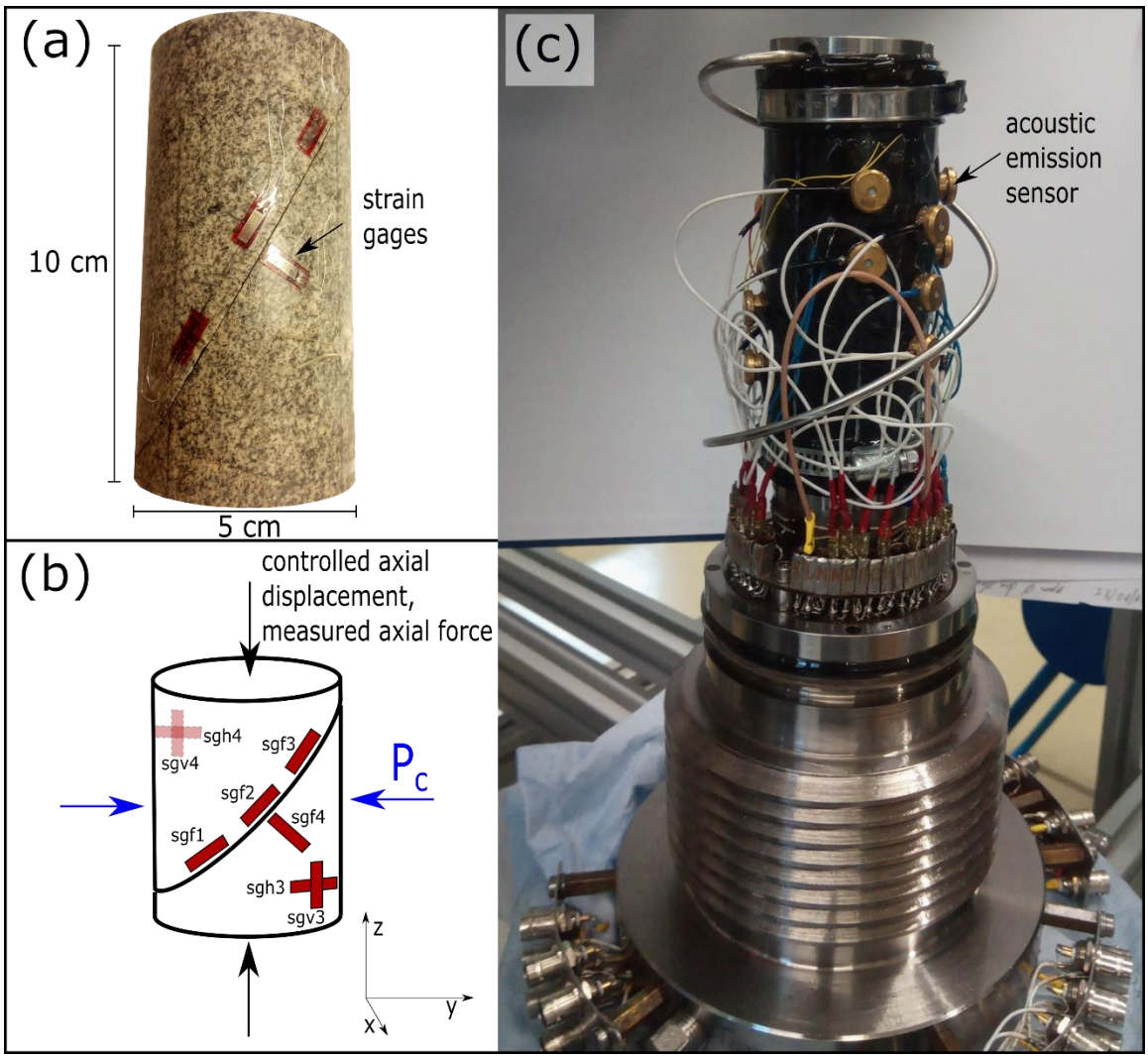

Figure S1. (a) Photography of the sawcut granite blocks with the strain gages glued directly on the sample. (b) Schematic view of the strain gages configuration and of the loading forces. (c) Specimen assembly with the AE sensors placed in brass casings mounted directly on the sample by filling holes pierced through the rubber jacket.

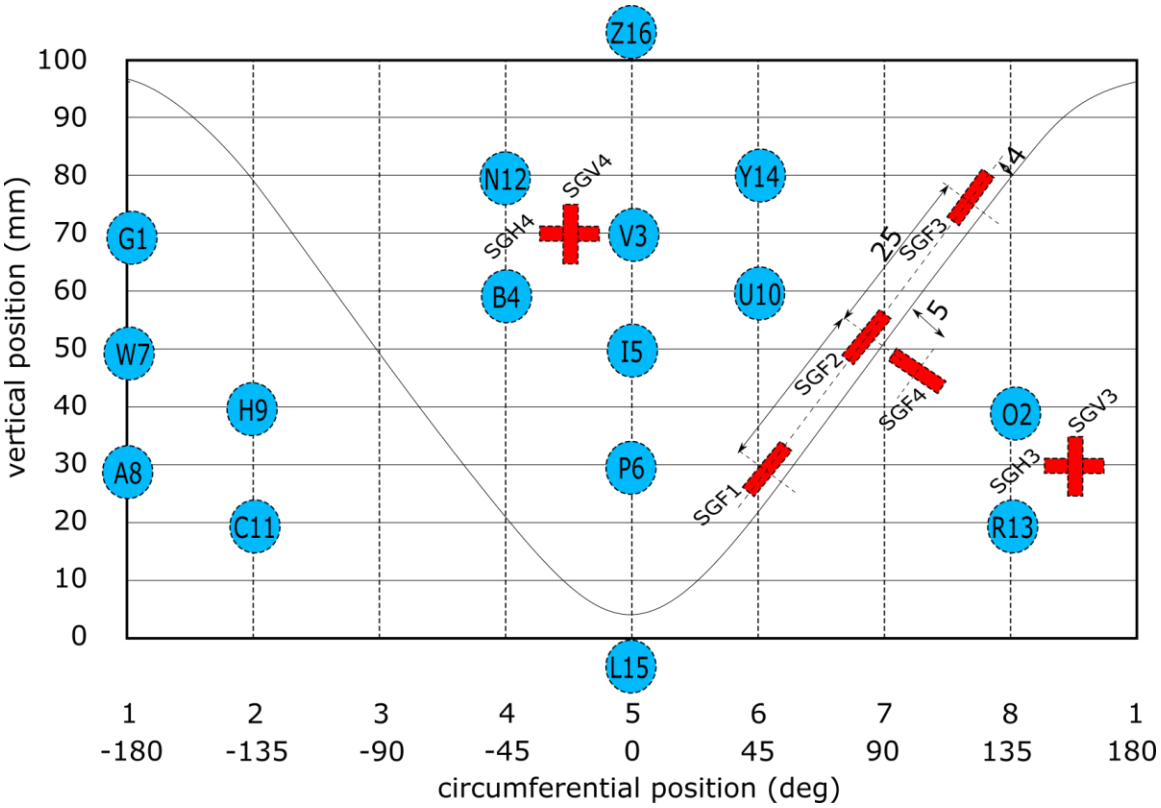

Figure S2. Sensor map with blue circles corresponding to the acoustic sensors array, and the red rectangles referring to the strain gages.

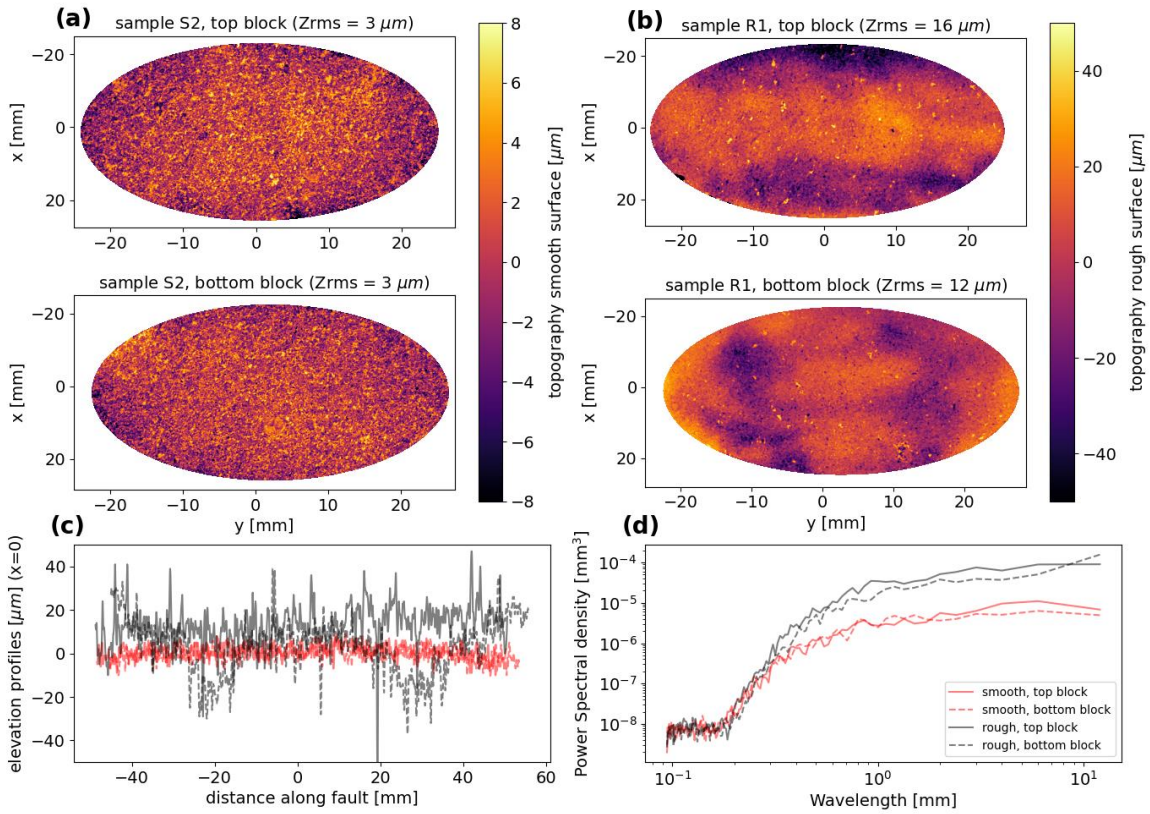

Figure S3. (a) Surface topography of top and bottom blocks for a smooth fault, sample S2. (b) Surface topography of top and bottom blocks for a rough fault, sample R1. (c) Elevation profiles along the fault surfaces major axis (at x=0) for the rough and smooth faults, top and bottom blocks. (d) Spectral analysis of the elevation profiles.

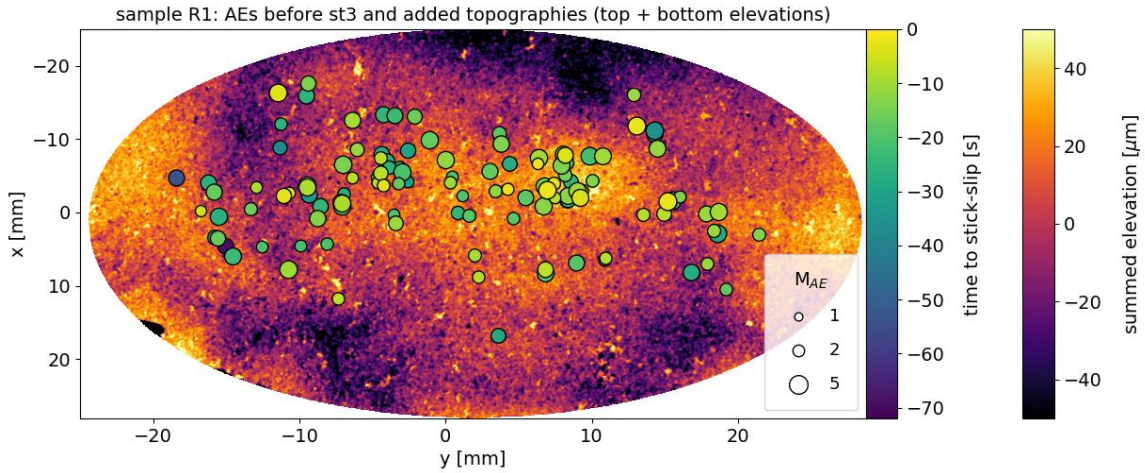

Figure S4. Added topographies of the rough surfaces from sample R1 (top block topography + bottom block topography) with superimposed acoustic emissions before stick-slip event st3.

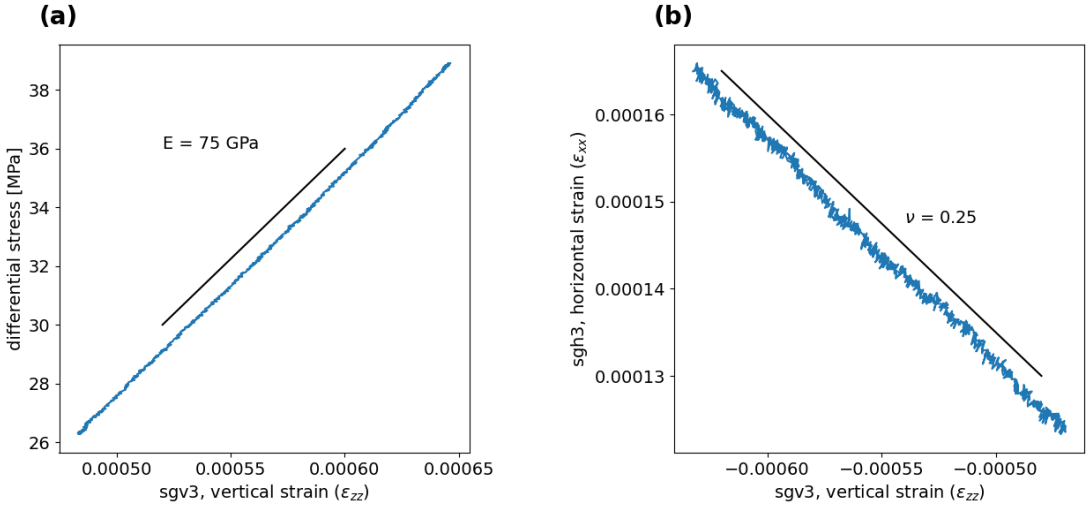

Figure S5. Elastic parameters estimates for La Peyratte granite samples, during elastic loading: (a) Young's modulus and (b) Poisson's ratio.

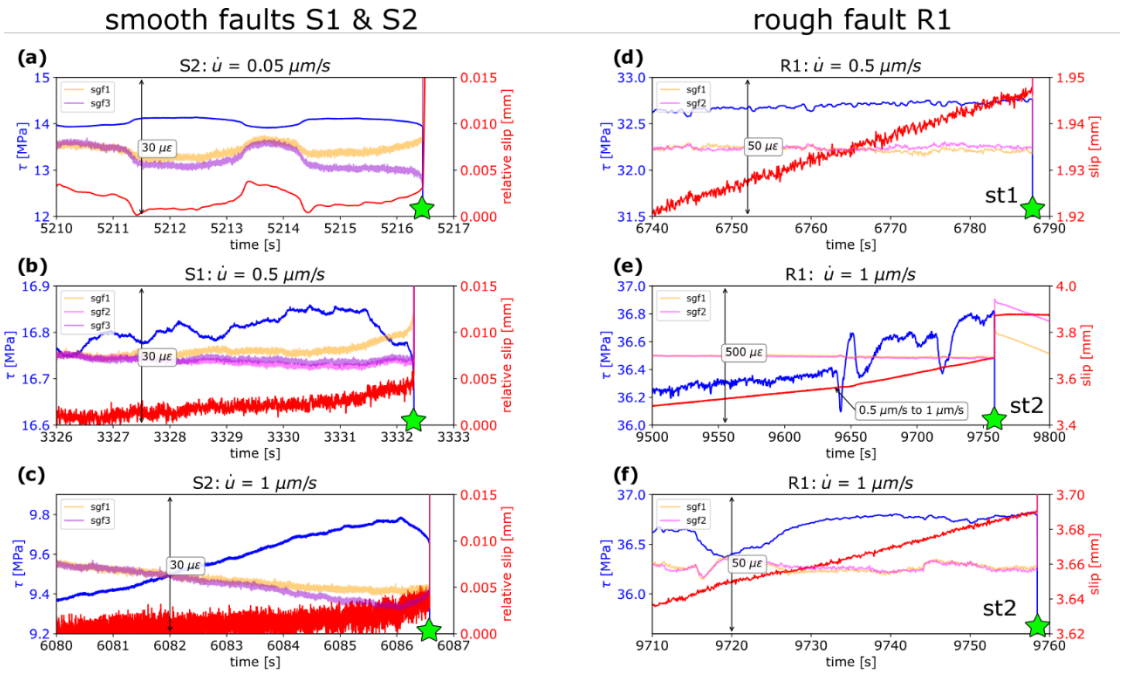

Figure S6. Evolution of shear stress (blue curve), slip (red curve) and available fault parallel strain gage signals (purple, pink and yellow curves), during a few seconds prior to stick-slip events for the smooth faults (a, b & c), and during a few tens of seconds prior to stick-slips events for the rough fault (d, e & f). The green stars indicate the stick-slips onsets. The change of load point displacement rate, from 0.5 μm/s to 1 μm/s prior to st2, is indicated on subplot (e).

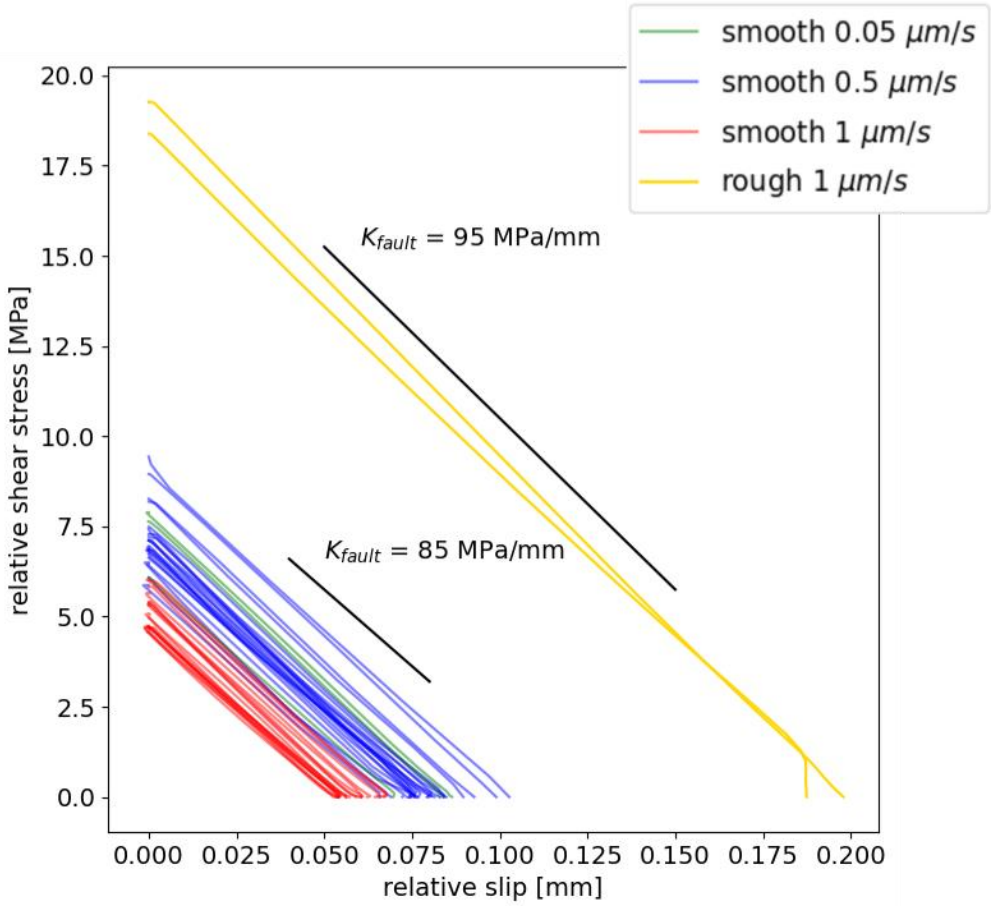

Figure S7. Shear stress versus fault slip (offset values), during stick-slip events for the smooth faults and the rough fault. The slopes corresponding to fault stiffness are indicated with solid black lines. The average fault stiffness K_{fault} is measured to be about $K_{fault} \approx 90$ MPa/mm. In addition, the axial stiffness of loading system K_{system} is estimated to be about $K_{system} = 1/(1/K_{sample} + 1/K_{machine}) = 229$ MPa/mm, where $K_{sample} = E / L = 750$ MPa/mm is the elastic stiffness of the sample with E and L being Young's modulus and sample length, respectively, and $K_{machine} = 330$ MPa/mm is the axial stiffness of loading machine. If we project fault slip and shear stress along the cylinder axis (z axis), along which loading forces are applied, we obtain a correcting factor c (i.e., $c = 1/(\sin\theta \times \cos^2\theta) = 2.66$, see equations (1) and (2)) for the equivalent axial stiffness of the fault. This results in the equivalent axial stiffness of the faults between 226 and 252 MPa/mm, comparable to axial stiffness of loading system.

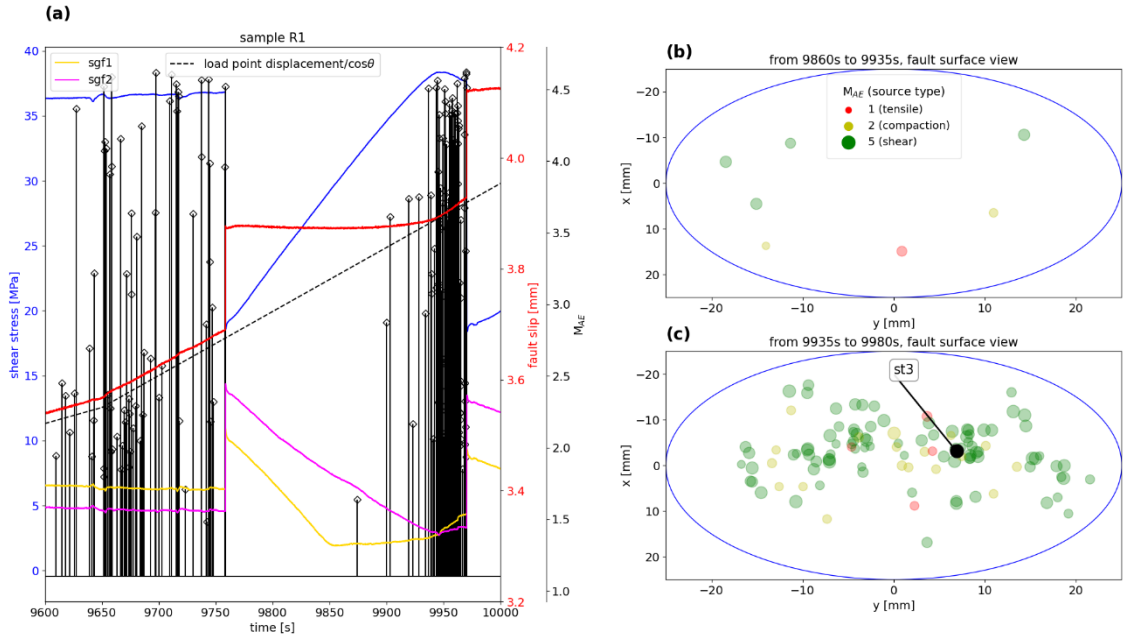

Figure S8. (a) Evolution of shear stress, slip, AEs and strain signals prior to stick-slip events st2 and st3 for sample R1. The load point displacement is indicated at a dashed black line. Loading point velocity was manually increased from 0.5 μm/s to 1 μm/s at t = 9650 s. (b) Locations of AE events occurring in the time window between t=9860 s and t=9935 s during which local slip occurs only close to strain gage sgf1 (sgf1 is relaxing and sgf2 remains in compression). (c) Locations of AE events occurring in the time window between t=9935 s to t=9980 s that corresponds to the onset of relaxation for sgf2, until the emergence of stick-slip event st3.

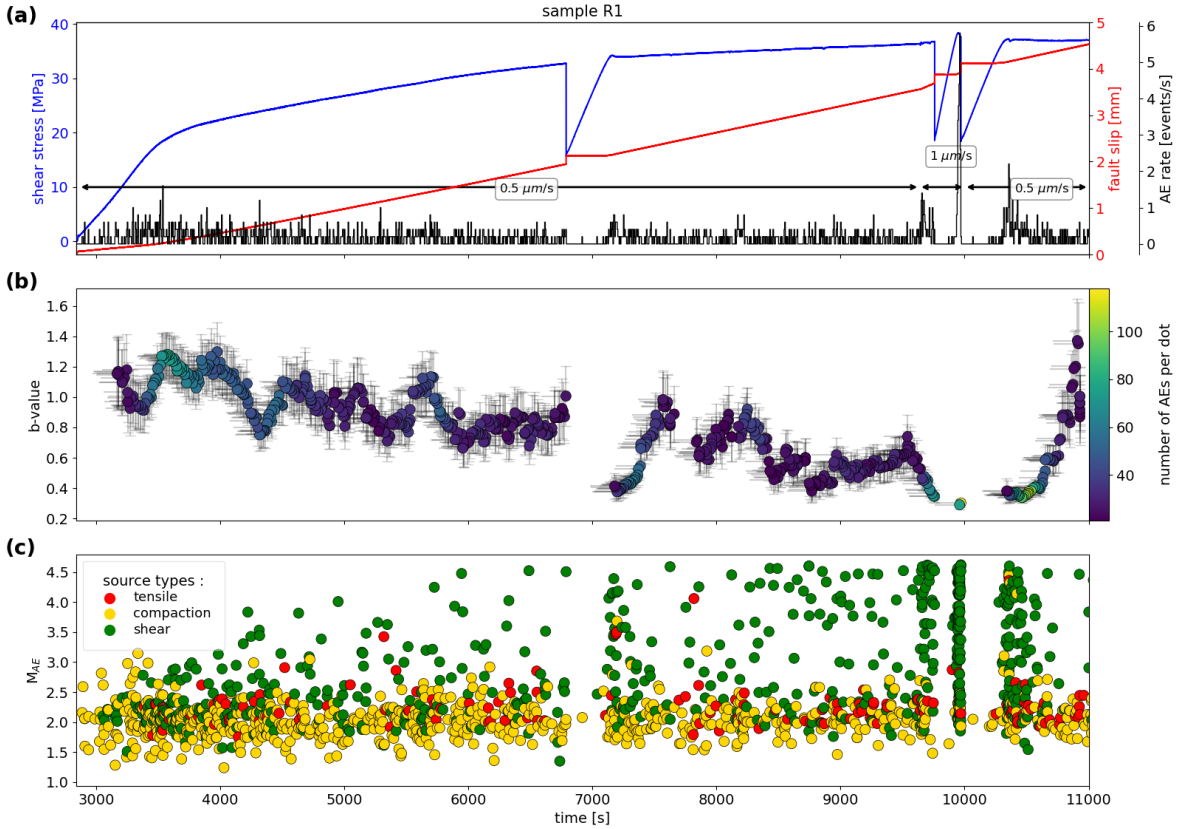

Figure S9. a) Evolution of shear stress, slip and AE rate for the rough sample R1. b) Evolution of *b*-value from AEs recorded on sample R1. The time windows for *b*-values calculations are indicated by horizontal grey lines, and the number of events during a time window is indicated on the color scale. Uncertainties are reported as vertical grey lines. c) Evolution of AE amplitude and type

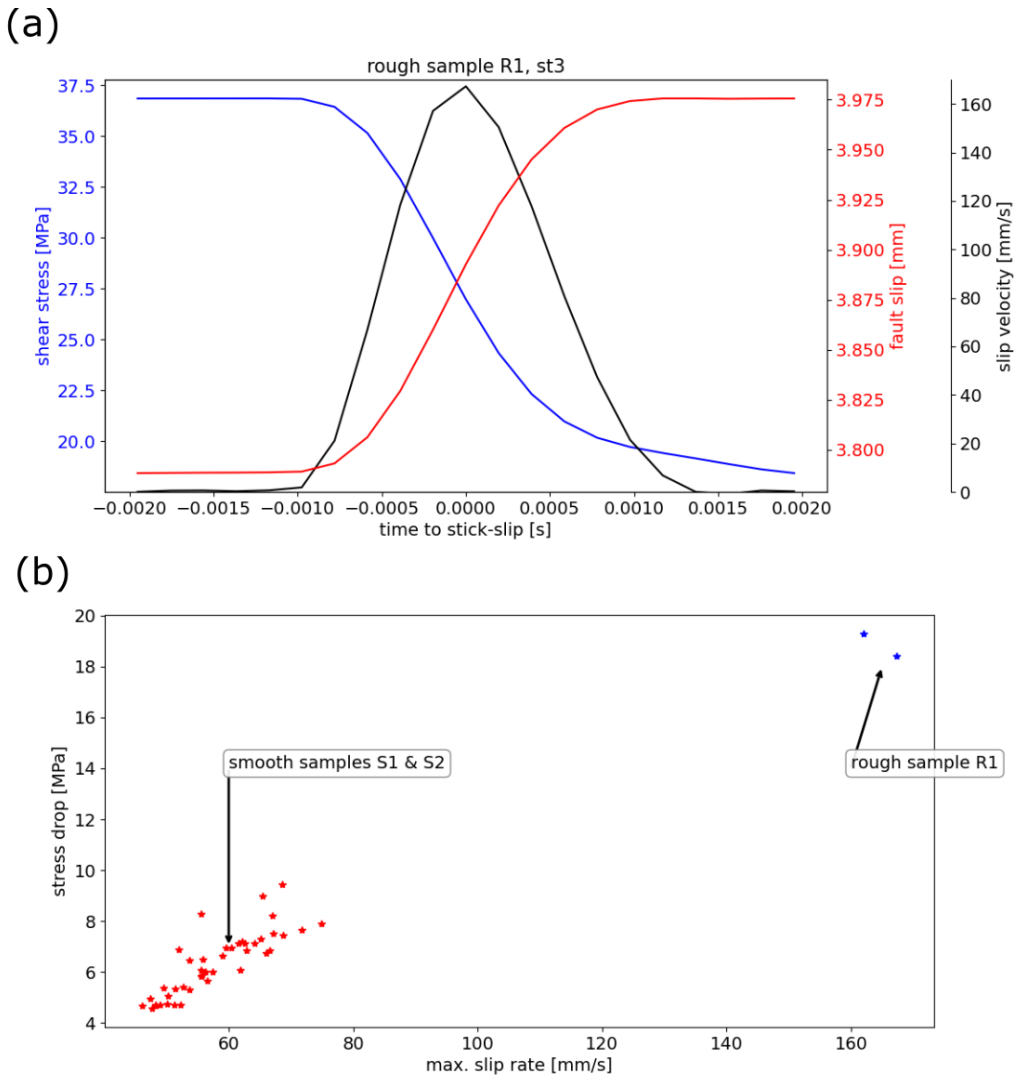

Figure S10. (a) Evolution of shear stress, slip and slip velocity during stick-slip event st3 on the rough fault R1. (b) Stress drop vs. maximum slip velocities during stick-slip events on smooth and rough faults.

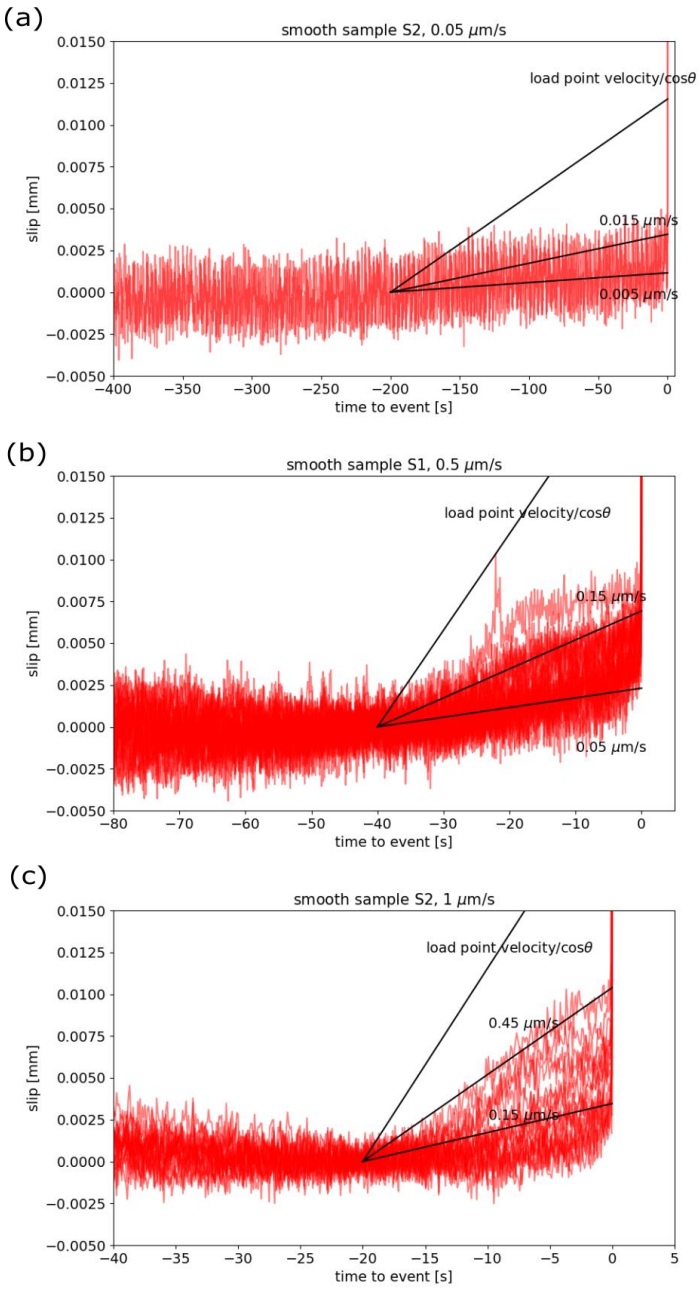

Figure S11. Preparatory slip prior to stick-slip events on smooth faults, and comparison with the load point velocities at (a) 0.05 µm/s with slip offset to zero 200 s before the events, (b) 0.5 µm/s with slip offset to zero 40 s before the events, and (c) 1 µm/s with slip offset to zero 20 s before the events.